RESEARCH ARTICLE

International Journal of Multidisciplinary and Scientific Emerging Research

Available at http://www.ijmser.com/ (ISSN 2349 – 6037)

Optical, Surface Morphological, And Antibacterial Properties of Nanostructured Tio_2:M (M=Fe, Ce, Ag) Thin Films

F. E. Ghodsi[*1], H. Dadvar[1] and G. Khayati[2]

[1]Department of Physics, Faculty of Science, University of Guilan, Rasht, **Iran**
[2]Department of Chemical Engineering, Faculty of Engineering, University of Guilan, Rasht, **Iran**

Accepted **30** September 2014, Available online **16** October 2014, **Vol.3, No.1 (October 2014)**

Abstract

In this research, undoped and doped (Fe, Ce, and Ag) antibacterial coatings of nanostructured TiO_2 films were prepared by a sol-gel dip coating method. Doped and undoped TiO_2 films were excited with ultraviolet (UV) radiation to improve their photo catalytic activity. The antibacterial activity against Staphylococcus Aureus bacteria was studied using an antibacterial–drop test and colony count method. The Fe doped TiO_2 films exhibited higher antibacterial activity than other samples. The percent of bacteria killing or killed (PBK) on bare glass substrate, undoped, Ce, Ag, and Fe doped TiO_2 thin films (after UV illumination) were 23.8, 50.3, 57.8, and 70.1%, respectively. Uv-Visible Spectrophotometry, Photoluminescence (PL), X-ray Diffraction (XRD), and Atomic Force Microscopy (AFM) were carried out to study the relation between optical, luminescence, structural, and surface morphological characteristics of the samples with their antibacterial activities. Several parameters such as thickness of the films, porosity in the films, crystallization, and surface morphology affect the antibacterial activity of transition metal doped TiO_2 thin films.

Keywords: *Titanium oxide, Optical properties, Surface morphology, XRD, Antibacterial.*

1. INTRODUCTION

In recent times, TiO_2 based composite and doped TiO_2 have received attention due to their applications in electro chromic devices [1, 2], gas sensor [3], photo catalyst [4], micro-integrated photonic devices [5]. Titanate (TiO_2) is an important semiconductor with wide band gap near 3.2eV, so it is just can be excited with ultra violet (UV) radiations that lead to photo catalytic properties [6-8]. Some researchers follow different ways named band gap engineering to change band gap energy [9, 10]. For this purpose, they use metal doping such as iron, silver, copper and cerium to change band gap energy and they found that excitation process also can occur with low energy illuminations such as sun light and florescent, or any visible lamps for doping [8].

Because of photo catalytic properties, TiO_2 can be used for antibacterial and self cleaning goals and its nanostructured films are also one of the well-known products for antibacterial properties [11-14]. Commonly, after irradiation by UV source a photo generated hole-electron pair is created. This hole-electron pair reacts with O_2 and H_2O that lead to cleaning agents on the surface of the samples. Then •OH and •OOH (radical species) can decompose with large organic molecules such as bacteria and tumour cells that lead to smaller elements. The combination of photo catalysis and super-hydrophilicity allows dirt wash with water [6, 11]. There are many processes to prepare nanostructured films that are applicable on the antibacterial surfaces. Among them, the sol-gel method is the most favourite because of the special advantages such as relatively low temperature process and more uniform phase distribution [11, 12, and 15].

In this paper, we prepared TiO_2 nanostructured thin films without and with different metal doping elements such as iron (Fe), cerium (Ce) and silver (Ag) via sol-gel method and investigate their antibacterial properties by antibacterial-drop test and colony count method [15, 16]. Then, we study the physical characteristics of samples to explain the relationship between physical properties and antibacterial activates with different analyses such as atomic force microscopy, scanning electron microscopy, X-Ray diffraction and photoluminescence spectroscopy.

2. EXPERIMENTAL PROCEDURE

2. 1. Samples Preparation

Undoped, Fe, Ce, and Ag doped TiO_2 films were deposited on glass substrates by dip coating technique at 116mm/min. withdraw speed from a sol-gel solution obtained by the hydrolysis of tetra-n-butylorthotitanate in ethanol and in the presence of HNO_3 acid as precursors, solvent, and catalyzer, respectively. $Fe(NO_3)_3.9H_2O$,

$Ce(NO_3)_3.6H_2O$, and $AgNO_3$ then added into the solution as Fe, Ce and Ag precursors. For all metal doped TiO_2, the molarities of solutions were equal and kept 0.1 mol/lit. in the sol-gel process. Before deposition, the glass substrates were first degreased by detergent, rinsed thoroughly by deionized water. Then, the substrates were cleaned ultrasonically in a mixture of ethanol and acetone (each of 50% in volume) for 15min. After that, the cleaning process was repeated with deionized water in ultrasonic cleaner. Next, the substrates were dried in an oven at 100°C for 30min. Finally, the substrates exposed to nitrogen gas. Three sets of films with different thicknesses were deposited by dipping substrates into the solutions for one, two and four times. The samples were dried in an oven at 150°C for 15min to evaporate the solvent and remove organic residuals and the coating process was repeated. Finally, the films were annealed in a furnace at 500°C for 2h in ambient condition.

2. 2. Samples Characterization

The optical properties of undoped and doped TiO_2 films were determined by photoluminescence (PL) measurements by using PerkinElmer (LS 55) Fluorescence spectrometer under excitation at 297nm. Surface morphology of the films was studied by Atomic Force Microscopy (AFM) using a Dual Scope Microscope model DME 2401. X-ray diffraction pattern (XRD) of films carried out for crystallography properties by X-ray diffractometer (Philips X'pert-MPD, Netherlands) with Cu-Ka radiation at 1.5406Å wavelength (scan range = 10°–70°, scanning rate = 0.05 °/s, applied voltage = 40kV, current = 30mA). The antibacterial activities of undoped, Fe, Ce, and Ag doped TiO_2 films against *Staphylococcus Aureus* (*S. Aureus*) bacteria were studied using the so-called antibacterial drop-test. Eq. 1 was used to calculate the percent of bacteria killing for undoped and metal doped TiO_2 films:

$$PercentofBacteriaKilling = \frac{N_t - N_s}{N_t} \times 100 \quad (1)$$

where N_t and N_s are the number of counted alive bacteria on the surface of uncoated and coated film, respectively.

3. RESULTS AND DISCUSSION

Transmission spectra of four layers deposited undoped, Fe, Ce, and Ag doped TiO_2 thin films are shown in Fig. 1. The transmission spectra of the undoped and transition metal (Fe, Ce, Ag) doped TiO_2 films deposited on glass substrates demonstrated relatively different characteristic. The transmission of undoped and Ce doped TiO_2 thin films were about 67 and 68% at wavelengths near 800nm and gradually increased at short wavelengths until they reached the values of 77 and 72% at around 400nm, respectively. For Fe and Ag doped TiO_2 thin films, transmission were about 72 and 71% at wavelengths near 800nm and steadily decreased at short wavelengths until they reached the values of 62 and 65% at around 400nm, respectively. The transmission of undoped, Ce, and Ag doped TiO_2 thin films first significantly rose at shorter wavelengths, and then decreased rather rapidly, at last approached zero at around 300nm. On the other hand, the transmission of Fe doped TiO_2 thin film gradually dropped at shorter wavelengths from 900 to 350nm, and then reduced quite quickly, at last approached zero at around 300nm. The rapid reduction below 360nm was because of the absorption of light caused by the excitation of electrons from the valence band to the conduction band. Indeed, the absorption edge of TiO_2 should be about 388nm because the band gap of TiO_2 is 3.2eV [4]. Nevertheless, this pseudo-blue shift of the absorption edge can be attributed to the quantum confinement effect appears in TiO_2 thin films deposited by sol-gel method because the crystallite size in them are smaller [4]. For Ag doped TiO_2 thin film, the absorption edge shifted towards shorter wavelengths and indicated an increase in the band gap of TiO_2 when it was doped with Ag. The absorption edge shifted towards longer wavelengths for Fe doped TiO_2 thin film resulting red shift when it was doped with Fe. Further absorption edge shift towards longer wavelengths was observed for Ce doped TiO_2 thin film due to additional reduction in band gap as a consequence of further red shift. The differences in transmission between the undoped and transition metal doped TiO_2 films can be attributed to the difference in absorption of light and thickness of the films.

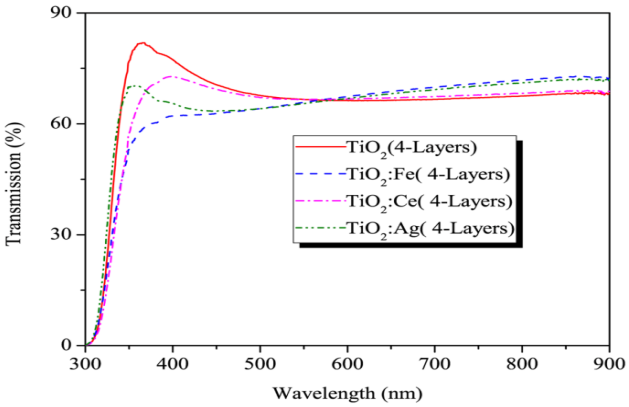

Figure 1: Transmission spectra of four layers deposited undoped and M (M = Fe, Ce, Ag) doped TiO_2 thin films.

The microstructure (such as electronic state, defect state, and energy level structure) of solids efficiently affects the optical properties of them [17]. The transfer behaviour of the photoinduced electrons and holes can be connected to the PL spectra. Hence, the PL spectra reveal the separation and recombination of photoinduced charge carrier which can be used principally to estimate the recombination rate of charge carriers [18].

Fig. 2 illustrates the emission spectra of TiO_2 films (undoped, Fe, Ce, and Ag doped) with an excitation wavelength of 300nm recorded at room temperature. The peak at 375, 374, 373, and 371nm for undoped TiO_2, Ce-doped TiO_2, Ag-doped TiO_2, and Fe-doped TiO_2 which are engendered by electron transition from the conduction

(CB) to valence band (VB) on base of the band gap energy [19]. In the cases of Ce and Fe-doped TiO_2, the peaks located at 378 and 398nm, respectively, may be caused by the vibration energy level in the CB and VB or free exciton absorption band around CB and VB [20]. The cooperation transition metal ions lead to narrowing of the band gap and greatly improve the photocatalytic activity in the visible light region. There is a considerable higher emission peak located at about 428 and 435nm in the case of Ce doped TiO_2 film with respect to other samples. It is attributed to the oxygen related defects such as oxygen vacancies in CeO_2. Another reason for this strong intensity is the crystallization of ceria into TiO_2 anatase lattice which is in consistence with XRD results. The very weak PL peaks located at 459 (for undoped), 463 (for all samples except Ce-doped), 473 (for Fe and Ag-doped), 485 (for all samples except Ce-doped) and 533nm (for undoped and Ce-doped) are most probably originated from the impurity or oxygen vacancies-related centres [21].

There is a broad line centred at approximately 586nm with two fine structures at 579 and 598nm corresponding to Ti interstitial as the origin of the carriers, the radiative recombination of electrons via intrinsic surface states of TiO_2, and transition assisted by three-phonon replica of impurity-related centres [21, 22], respectively. For the Fe-doped TiO_2, the yellow emission (emission in 586nm) has been decreased gradually with respect to Ce-doped TiO_2 and drastically in comparison with undoped TiO_2. For Ag-doped TiO_2 with respect to undoped TiO_2, the band is even lowered. It is supposed that these emissions are expected to originate from magnetic dipole transition. It is interesting to note that Fe, Ce, Ti, and Ag are ferromagnetic, paramagnetic (the magnetic susceptibility of cerium is higher than titanium), and diamagnetic elements. Hence, it can be deduced that the recombination efficiency of the Ce and Fe-doped TiO_2 are relatively slow which is probably the reason of the photocatalytic activity increasing in these sample. On the other hand, the PL intensity of Ag-doped TiO_2 is lower than pure TiO_2. Ag ions are diffused into the crystal lattice of TiO_2 and can act as traps to capture the photoinduced electron, causes retarding of the recombination of electron–hole pairs [23].

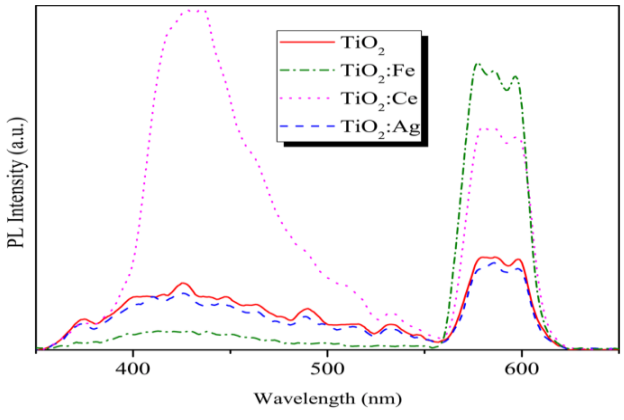

Figure 2: Emission PL spectra (λ_{ex}=297 nm) of the undoped and doped TiO_2 film.

According to XRD patterns in the Fig. 3, the undoped and doped TiO_2 films have nanocrystalline structures at the directions of (101) for anatase TiO_2. The Ce-doped TiO_2 thin films show two additional peaks of (200) and (220) that are corresponded to anatase and rutile phases of TiO_2, respectively. The Fe-doped TiO_2 thin films exhibit four additional peaks. Two peaks of (111) and (002) are attributed to brookite and rutile phases of TiO_2. In addition, a mixture of two crystalline phases, ilmenite ($FeTiO_3$) and pseudobrookite (Fe_2TiO_5) are identified for Fe-doped TiO_2 thin films. For Ag doped TiO_2 thin films, no peaks corresponding to either Ag or Ag_2O appear in X-ray diffraction pattern, indicating that no detectable secondary phase exists in anatase phase of pure TiO_2 thin films and Ag ion is incorporated well at the Ti lattice site.

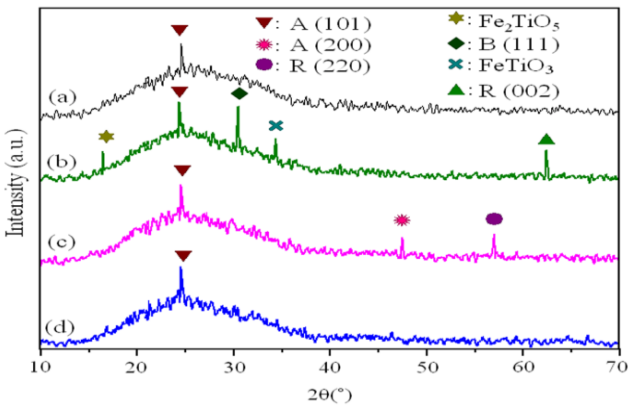

Figure 3: X-Ray diffraction pattern of undoped, Fe, Ce, and Ag doped TiO_2 films. A: anatase, R: rutile, B: brookite.

The grain sizes for each directions and phases have been calculated from the XRD patterns using the Sherrer's formula [24]:

$$D = \frac{0.94\lambda}{\beta Cos\theta} \qquad (2)$$

Where D is the grain size of crystallite, λ is the wavelength of X-rays used, β full width at half maximum (FWHM) of the diffraction peak and θ is the Bragg diffraction angle. The average grain size were calculated about 38, 63, 66, and 41nm for undoped, Fe, Ce, and Ag doped TiO_2 thin films, respectively.

Fig. 4 shows the atomic force microscope images of the dip coated undoped and doped TiO_2 films annealed at 500 ºC. The images show porous structures in micro and nano scales which we named them as Caldera Volcano Shape Porous (CVSP) due to their similarity to Caldera volcano. These type porous structures may be formed due to fast drying in the interval of deposition process and then annealing at high temperature (500ºC). Thus, a solute gel formed during each drying process and when the films annealed at last, the solute gel remove similar to molten volcano. As can be seen in Fig. 4, for Fe doped TiO_2 thin films CVSP in micro and nano size is higher than other samples and for Ce doped TiO_2 thin films just nano size CVSP is more than other samples. The type and size of porosity changes the surface area of the sample which can

play important role in its antibacterial activity. The detail illustrations of Fig 4b with four different scales porous were given in Fig. 5. In the inside (Fig. 5c) and next to outside (Fig. 5d) edge of volcano (Fig. 5a), there are CVSP`s about 22 and 31nm, respectively. There are several porous on the plateau CVSP`s about 32nm. Table 1 gives some morphological information such as root mean square roughness, (R_{RMS}), average void diameter (V_{AD}), rate of void to material (V_{AM}), and average breadth of voids (V_{AB}) about the samples.

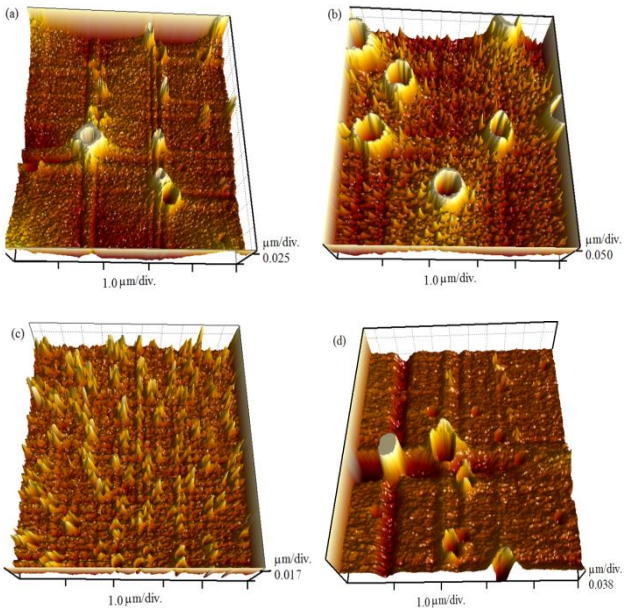

Figure 4: AFM micrographs of the (a) undoped, (b) Fe, (c) Ce, and (d) Ag doped TiO_2 films.

In order to survey the antibacterial properties of doped TiO_2 films on *S. Aureus* bacteria, bactericidal effect assay was performed by two methods: the antibacterial-drop test and the colony count method. *S. Aureus* PTCC 1431 was used as the experimental bacteria and cultured on the culture medium at 37°C for 18–24h. The cultured bacteria were added in 10 ml. saline solution to reach the approximate concentration of 10^8CFU/ml. A portion of the saline solution containing the bacteria was diluted to 10^6

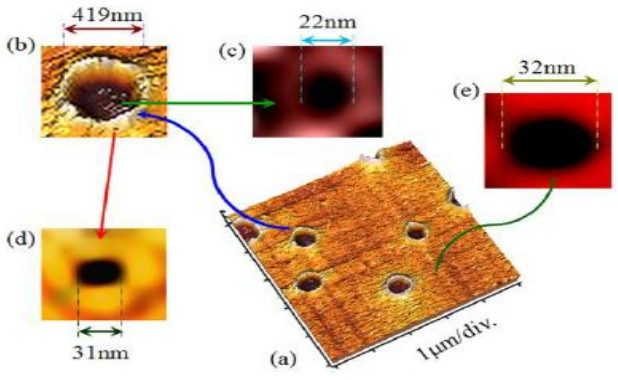

Figure 5: AFM micrographs of Fe doped TiO_2 films with details of CVSP in different scales.

CFU/ml for the "drop-method" antibacterial experiments. The samples were placed in the sterilized Petri dishes and then 100µl of saline solution with bacteria was added drop wise onto the surface of each film. The surface of the samples was covered by an ant-staling film. The samples were laid at ambient temperature for 5h. After this process, the bacteria that containing drops were washed from the surface of the films by 5ml phosphate buffer solution (PBS) in the sterilized Petri dish. In the next step, 10µl of each bacteria suspension was dispersed on the culture medium. The numbers of surviving bacteria on the Petri dishes were counted after incubation for 24h. at 37°C.

Fig. 6 shows the results of antibacterial drop-test for bare glass substrate, bare glass substrate irradiated with UV, undoped, Ag doped, Ce doped, and Fe doped TiO_2 films, and *PBK*. As can be seen in the figure, the coated glass substrates reveal higher antibacterial activity than the uncoated glass substrate. In addition, the number of layers and the type of metal dopant play an important role with regards to the antimicrobial activity of the samples. The difference in *PBK* was 13, 11, 24 and 16% for undoped, Ce, Ag, and Fe doped TiO_2 films, respectively, when the number of deposited layers increased from 1 to 4. On the other hand, The *PBK* for the four layers deposited films (Fig. 6c) were 23.8, 50.3, 57.8, and 70.1% for undoped, Ce, Ag, and Fe doped TiO_2 thin films. The highest *PBK* (70%) and *S.Aureus* reduction was observed for the four layers deposited Fe doped TiO_2 film.

Sample	*d* (nm)	R_{RMS} (nm)	V_{AD} (nm)	V_{AM} (%)	V_{AB}(nm)
TiO_2	153	1.54	76.2	31	74.9
TiO_2:Fe	196	3.25	92.0	73	88.1
TiO_2:Ce	124	1.13	74.1	14	71.3
TiO_2:Ag	172	1.78	79.8	41	81.6

Table 1: The film thickness (*d*), root mean square roughness (R_{RMS}), average void diameter (V_{AD}), rate of void to material (V_{AM}), and average breadth of voids (V_{AB}) for samples.

The increase in photocatalytic activity with transition metal doping is correlated to a shift in the optical absorption of the catalyst in the visible region. TiO_2 absorbs only UV energy (below 3.2eV) while transition metal doped catalyst absorbs UV and a portion of visible energy hence there is increase in photocatalytic activity. Existence of pores on the surface of the films is another reason to increase of photocatalytic activity of doped TiO_2 thin films. The increase in the number of pores enhances the hydroxyl content of the films. When a semiconductor is illuminated it generates electrons (e^-) and holes (h^+) in heterogeneous photocatalysis. The holes (h^+) and OH^- ions are combined and hydroxyl radicals ($h^+ + OH- \rightarrow \bullet OH$) are formed generating strong oxidizing conditions. The formation of surface hydroxyl radical on the surface of the photocatalyst is oxidizing sample which eventually

influences the photocatalytic activity. Therefore, increasing of the hydroxyl content of the films enhances the photocatalytic activity [25] and antibacterial activity of samples, consequently.

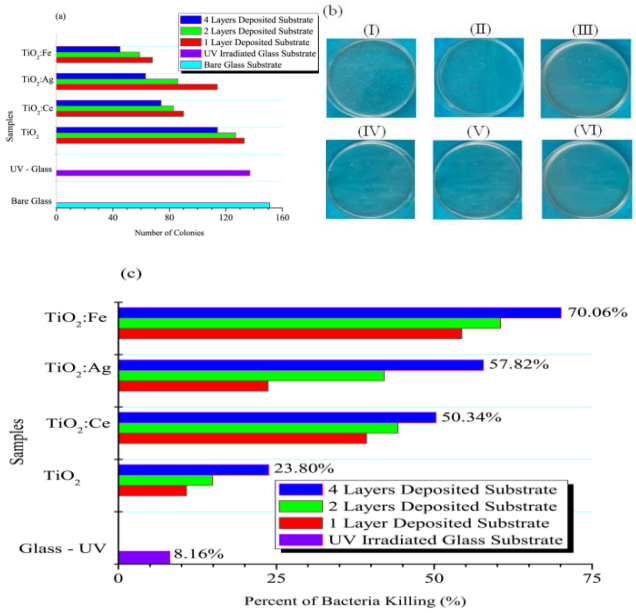

Figure 6: Results of antibacterial drop-test: (a) number of colonies, (b) antibacterial activity in Petri dishes for different doped TiO_2 films: (I) bare glass substrate, (II) bare glass substrate irradiated with UV, (III) undoped (IV), Ag-doped (V), Ce-doped, and (VI), Fe-doped TiO_2 film, and (c) percent of bacteria killing (*PBK*).

4. CONCLUSIONS

For antibacterial activity investigation against *Staphylococcus Aureus* bacteria two methods were used. One of them was antibacterial-drop test and other colony count method. The doped TiO_2 films deposited on the glass substrates by sol gel process exhibited good antibacterial activity under ultraviolet light radiation. Doping of transition metal leads to improve antibacterial activity of TiO_2 thin films. Various factors such as surface morphology, structure, porosity in films, crystallization, thickness of the films, and surface roughness influence the antibacterial activity of the TiO_2 thin films. Fe doped TiO_2 film with higher porosity, thickness, and surface area that lead to high percent of bacteria killing near 70%, because of its high photo catalytic properties.

ACKNOWLEDGEMENTS

The authors would like to acknowledge the University of Guilan Research Council for the support of this work.

REFERENCES

[1] Ghodsi F.E., Tepehan F.Z. (2006), Investigation on the optical and structural properties of spin coated CeO_2–TiO_2 thin films, *Physica Status Solidi (a)* Vol. 203, pp. 526–533

[2] Ghodsi F.E., Tepehan F.Z., Tepehan G.G. (2008), Electrochromic properties of heat-treated thin films of CeO_2–TiO_2–ZrO_2 prepared by sol–gel route, *Solar Energy Materials and Solar Cells* **,** Vol. 92, pp. 234–239.

[3] Wisitsoraat A., Tuantranont A., Comini E., Sberveglieri G., Wlodarski W. (2009), Characterization of n-type and p-type semiconductor gas sensors based on NiOx doped TiO_2 thin films, *Thin Solid Films*, Vol. 517, pp. 2775–2780.

[4] YU J., YU J.C., CHENG B., ZHAO X. (2002), Photocatalytic activity and characterization of the sol-gel derived Pb–doped TiO_2 thin films, Journal *of Sol–Gel Science and Technology*, Vol. 24: 39–48.

[5] Ting C.C., Chen S.Y., Lee H.Y. (2003), Physical characteristics and infrared fluorescence properties of sol–gel derived Er^{3+}–Yb^{3+} codoped TiO_2, *Journal of Applied Physics*, Vol. 94, pp. 2012–2019.

[6] Dadvar H., Ghodsi F.E., Dadvar S. (2012), in Synthesis, properties, and applications of special substrates coated by titanium dioxide nanostructured thin films via sol–gel process, In: *Advanced methods and applications in chemoinformatics: research progress and new applications*. Castro E.A.; Haghi A. K. Eds.; Hershey, PA, IGI Global Publisher, pp. 246–279.

[7] Dadvar S., Tavanai H., Dadvar H., Morshed M., Ghodsi F.E. (2011**),** Uv–protection and photocatalytic properties of electrospun polyacrylonitrile nanofibrous mats coated with TiO_2 nanofilm via sol–gel, *Journal of Sol–Gel Science and Technology*, Vol. 59: pp. 269–275.

[8] Senthil T.S., Muthukumarasamy N., Agilan S., Thambidurai M., Murthy K.V.R., Balasundaraprabhu R. (2009), Structural investigations on nanocrystalline TiO_2 thin films prepared by sol-gel spin coating technique, *Journal of Optoelectronic and Advanced Materials*, Vol. 11, pp. 831–833.

[9] Long R., English N.J. (2009), Band gap engineering of (N, Ta) –codoped TiO_2: a first principles calculation, Chemical *Physics Letters*, Vol. 478, pp. 175–179.

[10] Long R., English N.J. (2009), First–principles calculation of nitrogen–tungsten codoping effects

on the band structure of anatase–titania, *Applied Physics Letters*, Vol. 94, pp. 1321021–1321023.

[11] Sunada K., Watanabe T., Hashimoto K. (2003), Studies on photokilling of bacteria on TiO_2 thin film, *Journal of Photochemistry and Photobiology A: Chemistry*, Vol. 156, pp. 227–233.

[12] Mai L., Wang D., Zhang S., Xie Y., Huang C., Z hang Z. (2010), Synthesis and bactericidal ability of Ag/TiO_2 composite films deposited on titanium plate, *Applied Surface Science*, Vol. 257, pp. 974–978.

[13] Aronniemi M., Lahtinen J., Hautojärvi P. (2004), Characterization of iron oxide thin films, *Surface and Interface Stresses*, Vol. 36, pp. 1004–1006.

[14] Chaisuk C., Wehatoranawee A., Preampiyawat S., Netiphat S., Shotipruk A., Panpranot J. Jongsomjit B., Mekasuwandumrong O. (2011), Preparation and characterization of CeO_2/TiO_2 nanoparticles by flame spray pyrolysis, *Ceramic International*, Vol. 37, pp. 1459–1463.

[15] Sun S.Q., Sun B., Zhang W., Wang D. (2008), Preparation and antibacterial activity of Ag–TiO_2 composite film by liquid phase deposition (LPD) method, *Bulletin of Materials Science*, Vol. 31, pp. 61–66.

[16] Jeon H.J., Yi S.C., Oh S.G. (2003), Preparation and antibacterial effects of Ag–SiO_2 thin films by sol–gel method, *Biomaterials*, Vol. 24, pp. 4921–4928.

[17] Zhang L., Mo C.M. (1995), Luminescence in nanostructured materials, *Nanostructed Matererials*, Vol. 6, pp. 831–834.

[18] Zhu Y.C., Ding C.X. (1999), Investigation on the surface state of TiO_2 ultrafine particles by luminescence, *Journal of Solid State Chemistry*, Vol. 145, pp. 711–715.

[19] Liu B., Wen L., Zhao X. (2007), The photoluminescence spectroscopic study of anatase TiO_2 prepared by magnetron sputtering, *Material Chemistry and Physics*, Vol. 106, pp. 350–353.

[20] Guo P., Guo L. (2010), Study on the optical properties, crystal growth and photo–catalytic activity of Ni–doped TiO_2 nanoparticles, In Proceedings of 18th World Hydrogen Energy Conference 2010–WHEC, *Energy & Environment*, pp. 601–608.

[21] Jin Y., Li G., Zhang Y., Zhang Y., Zhang L. (2002), Fine structures of photoluminescence spectra of TiO_2 thin films with the addition of $ZnFe_2O_4$, *Journal of Physics D: Applied Physics*, Vol. 35, pp. 37–40.

[22] Pal M., Pal U., Miguel J., Jiménez G.Y., Rodríguez F.P. (2012), Effects of crystallization and dopant concentration on the emission behavior of TiO_2:Eu nanophosphors, *Nanoscale Research Letters*, Vol. 7, Vol. 1-12.

[23] Tryba B., Piszcz M., Morawski A.W. (2010), Photocatalytic and Self-Cleaning Properties of Ag–Doped TiO_2, *The Open Material Science Journal*, Vol. 4, pp. 5-8.

[24] Patterson A.L. (1939), The Scherrer formula for X-Ray particle size determination, *Physical Review Letters*, Vol. 56, pp. 978–982.

[25] Sonawane R.S., Kale B.B., Dongare M.K. (2004), Preparation and photo-catalytic activity of Fe–TiO2 thin films prepared by sol–gel dip coating, *Material Chemistry and Physics*, Vol. 85, pp. 52–57.